Adiabatic Thermal Radiation Pumps for Thermal Photonics

Huanan Li,[1,2,*] Lucas J. Fernández-Alcázar,[1,*] Fred Ellis,[1] Boris Shapiro,[3] and Tsampikos Kottos[1]
[1]*Wave Transport in Complex Systems Lab, Department of Physics, Wesleyan University, Middletown, Connecticut 06459, USA*
[2]*Photonics Initiative, Advanced Science Research Center, CUNY, New York, New York 10031, USA*
[3]*Technion—Israel Institute of Technology, Technion City, Haifa 32000, Israel*

(Received 29 April 2019; published 15 October 2019)

We control the direction and magnitude of thermal radiation, between two bodies at equal temperature (in thermal equilibrium), by invoking the concept of adiabatic pumping. Specifically, within a resonant near-field electromagnetic heat transfer framework, we utilize an *instantaneous* scattering matrix approach to unveil the critical role of wave interference in radiative heat transfer. We find that appropriately designed adiabatic pumping cycling near diabolic singularities can dramatically enhance the efficiency of the directional energy transfer. We confirm our results using a realistic electronic circuit setup.

DOI: 10.1103/PhysRevLett.123.165901

Introduction.—Understanding the rules that dictate thermal radiation and the development of novel schemes that allow us to tame its flow has offered over the years an exciting arena of research [1–4]. From one side, there are fundamental challenges associated with basic constraints that need to be understood in order to manage thermal radiation [4–8]. At their core are questions associated with the importance of thermal electromagnetic fluctuations and their implications in directional thermal radiation. On the other hand, there is a wide range of applications that can benefit from advances in thermal radiation management. In fact, in close connection with the rapid developments that we are witnessing in the field of nanophotonics, the subfield of thermal photonics has emerged [9–20] and promises to revolutionize modern energy technologies. Examples include thermophotovoltaics [21–24], thermal imaging [25,26], thermal circuits [27–29], and radiative cooling [30].

In this Letter, we propose manipulating thermal radiation by introducing the concept of an adiabatic thermal radiation pump. The pump operates between two reservoirs that are maintained at the same temperature—as opposed to the common approach where heat flow requires a temperature gradient. A possible setup of a thermal radiation pump is depicted in Fig. 1(a). By slow periodic modulation of the eigenfrequencies of two resonators, coupled to two separate reservoirs at equal temperature T, one can transfer thermal radiation from one reservoir to the other (see green arrows). This process of creating a directional radiation flow may be termed *adiabatic thermal radiation pumping*. The amount of heat pumped in one cycle depends on the details of the modulation process. In particular, we show that the existence of a diabolic point (DP) (i.e., an exact degeneracy) [31] in the spectrum of the system's Hamiltonian leads to a dramatic enhancement of the effect, for an appropriately chosen modulation cycle. Our theoretical results are based on a coupled-mode-theory (CMT) approach to resonant thermal radiation and are backed up by detailed numerical simulations using realistic circuit setups; see Fig. 1(b). Our approach unveils the importance of wave interference in radiative heat transfer by connecting the pumped thermal radiative current with the instantaneous reflection phase. This connection opens up new possibilities in the field of thermal photonics. Our concept of the adiabatic thermal radiation pumping is inspired by adiabatic charge pumping in condensed matter, where a dc current in response to a slowly varying time-periodic

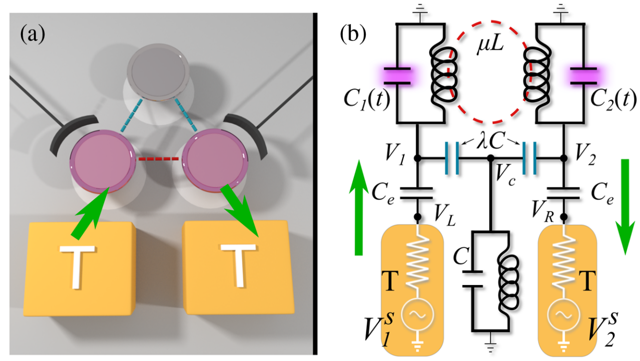

FIG. 1. Proposed implementations of our thermal radiation pumping scheme. (a) A nanophotonic structure consisting of three single-mode resonators. The resonant frequencies of the first and third resonators (purple colors) are periodically modulated via a weak adiabatic modulation of the permittivities of the resonators. The system is in contact with two independent baths at the same temperature T. (b) A circuit consisting of three LC resonators. Two of these resonators are modulated via their (purple) capacitances. The circuit is coupled capacitively to two artificial reservoirs at the same temperature T. The reservoirs are implemented by synthesized noise sources generating random voltages $V_{1,2}^s$ with a prescribed spectral distribution. The positive direction for the pumped flow is chosen to match the green arrows.

potential has been proposed [32–37] and experimentally demonstrated [38].

CMT modeling of thermal radiation.—We consider a photonic circuit supporting a finite number of resonant modes N_s described by a time-independent Hamiltonian H_0. The system is in contact, via leads, with two separate heat baths at constant temperature [see Fig. 1(a), where $N_s = 3$]. The system-lead coupling is described by an operator $\hat{W}$.

At thermal equilibrium, the baths generate photons at frequency ω with mean number $\Theta_T(\omega) = (e^{(\hbar\omega/k_B T)} - 1)^{-1}$ given by the Bose-Einstein statistics. The radiative thermal energy exchange between the two heat baths can be studied using a time-dependent CMT [39,40]

$$\imath \frac{d}{dt}\Psi = H_{\rm eff}\Psi + \imath \hat{W}\theta^{(+)}, \qquad H_{\rm eff} = \left(H_0 + \Lambda - \frac{\imath}{2}\hat{W}\hat{W}^T\right),$$
$$\theta^{(-)} = \hat{W}^T\Psi - \theta^{(+)}, \tag{1}$$

where $\Psi = (\psi_1, \psi_2, \ldots, \psi_{N_s})^T$ describes the modal amplitude of the field and it is normalized in a way that $|\psi_s|^2$ represents the energy of the sth mode. The variables $\theta_n^{(\pm)}(\omega)$ [frequency domain of $\theta^{\pm}$ in Eq. (1)] indicate the flux amplitudes of the incoming (+) and outgoing (−) waves from and towards the reservoir $n = 1, 2$ via leads. At thermal equilibrium, the incoming flux (from the reservoirs) satisfies the correlation relation [39]

$$\langle \theta_n^{(+)}(\omega)(\theta_m^{(+)}(\omega'))^* \rangle = \frac{\hbar\omega}{2\pi}\Theta_T(\omega)\delta(\omega - \omega')\delta_{nm}, \tag{2}$$

and therefore the outgoing power from the nth heat bath is given by the double integral over frequency ω of this correlation function.

The scattering matrix S, connecting the outgoing $\theta^-(\omega)$ to the incoming $\theta^+(\omega)$ waves, is evaluated using Eq. (1). We have [41]

$$S = -I_2 - \imath W^T G_{\rm eff} W, \qquad G_{\rm eff} = \frac{1}{H_{\rm eff} - \omega I_{N_s}}, \tag{3}$$

where I_n is the $n \times n$ identity matrix. The $(N_s \times 2)$-dimensional matrix W describes the coupling to the leads (in frequency domain). Its elements are $W_{s,n} = \sqrt{v_g} w_n \delta_{sn}$, where w_n are dimensionless coupling strengths, and $v_g = \partial\omega(k)/\partial k$. Finally, the renormalization matrix Λ in Eq. (1) originates from the coupling of the system with the leads, and it is specific to the properties of the leads.

Thermal radiation pumps.—Next, we consider a system whose Hamiltonian $H_0(u^t, v^t)$ depends on two time-varying independent parameters (u^t, v^t) [42]. We assume that these parameters are periodically modulated in time with frequency Ω such that $H_0(t) = H_0(t + 2\pi/\Omega)$. During one period of the modulation, these parameters form a closed cycle in the (u^t, v^t) parameter space. The associated enclosed "pumping area" is $\mathcal{A} \equiv \int_0^{2\pi/\Omega} dt u^t (dv^t/dt)$. We consider circumstances where the (u^t, v^t) variations are small such that $\mathcal{A} \to 0$.

We will evaluate the radiative (time-averaged) thermal energy flux per pumping area $\bar{\mathcal{I}}$, from one bath to another during one pumping circle. The latter is

$$\bar{\mathcal{I}} \equiv \frac{\Omega}{2\pi}\int \frac{d\omega}{2\pi}\hbar\omega\Theta_T(\omega)Q(\omega),$$
$$Q(\omega) \equiv \lim_{\mathcal{A}\to 0}\frac{\int_0^{\frac{2\pi}{\Omega}} dt \mathcal{I}_{x_0}(t, \omega)}{\mathcal{A}}, \tag{4}$$

where $Q(\omega)$ is the radiative energy density (i.e., per area in the parameter space) and $\mathcal{I}_{x_0}(t, \omega)$ is the dimensionless (normalized) time-dependent directional net energy current, at some observation cross section at $x = x_0$ within the leads. The latter is evaluated under the condition of two uncorrelated counterpropagating incoming waves of frequency ω and unit flux. In the case where H_0 is static, the thermal radiative current $\mathcal{I}$ at each lead is zero. From Eq. (4), it is clear that an understanding of $Q(\omega)$ is essential for the analysis and control of $\bar{\mathcal{I}}$ [44].

Adiabatic pumping.—In the adiabatic limit, $\Omega \to 0$, the study of radiative thermal energy $Q(\omega)$ boils down to the analysis of the *instantaneous* scattering matrix S^t [32]. The latter is given by Eq. (3), with the superscript t indicating the parametric dependence of the matrix elements of S at a specific instant t during the pumping cycle. It can be generally parametrized in terms of three independent parameters: the instantaneous reflectance R^t and the instantaneous reflection and transmission phases α^t, $\varphi^t \in \mathcal{R}$, respectively. Specifically, we have

$$S^t = e^{\imath\varphi^t}\begin{bmatrix} \sqrt{R^t}e^{\imath\alpha^t} & \imath\sqrt{1 - R^t} \\ \imath\sqrt{1 - R^t} & \sqrt{R^t}e^{-\imath\alpha^t} \end{bmatrix}, \qquad 0 \le R^t \le 1. \tag{5}$$

Using this parametrization, we write $Q(\omega)$ as [42]

$$Q(\omega) = \frac{1}{\omega}\frac{\partial(\omega P)}{\partial\omega},$$
$$P(\omega) = \lim_{\mathcal{A}\to 0}\frac{1}{\mathcal{A}}\int_0^{\frac{2\pi}{\Omega}} dt R^t \frac{d\alpha^t}{dt} = \left|\frac{\partial(R^t, \alpha^t)}{\partial(u^t, v^t)}\right|, \tag{6}$$

which applies whenever the period of the driving is larger than the time that the "photons" dwell inside the scatterer. We stress that Eq. (6) allows us to connect wave interference phenomena (imprinted via the reflection phase α^t) with the thermal radiation problem, thus opening up new directions in the field of thermal photonics. Using Eqs. (3) and (5), we have

$$R^t = |S_{11}^t|^2, \qquad \frac{d\alpha^t}{dt} = \frac{1}{2\imath}\frac{d}{dt}\left(\ln\frac{S_{11}^t}{S_{22}^t}\right), \tag{7}$$

where the subscripts indicate the matrix elements of S^t.

Substitution of Eq. (6) into Eq. (4) allows us to express $\bar{\mathcal{I}}$ as

$$\bar{\mathcal{I}} = \frac{\Omega}{2\pi}\int \frac{d\omega}{2\pi}\left(-\frac{\partial\Theta_T(\omega)}{\partial\omega}\hbar\omega\right)P(\omega, d, \{w_n\}), \quad (8)$$

where for near-resonant thermal radiation the boundary contributions (associated with the integration by part) are neglected. Note that the integral $\int_0^{2\pi/\Omega} dtR^t(d\alpha^t/dt)$ appearing in $P(\omega)$ plays a prominent role in the case of adiabatic *charge* pumping near zero temperature [32–37]. It was found that it can be quantized (in units of 2π) only when a significant portion of resonance line at the Fermi level is encircled [45–47]. This condition is not applicable in our case, where the quantity of interest is the pumping density defined in the limit of infinitesimally small pumping circle $\mathcal{A} \to 0$. At the same time, even in the adiabatic charged pumping framework, there are many circumstances where the quantization does not occur [45,46,48]. This discrepancy is related to the presence of the instantaneous reflectance $R^t(\omega)$, and thus this integral is generally not a topological number [49].

In the current framework of thermal radiation, the thermal energy flux density $\bar{\mathcal{I}}$ is more convoluted than the pumped electron charge. From Eq. (8), we see that $\bar{\mathcal{I}}$ involves a *weighted* integral of $P(\omega)$ where the weight, indicated by the large parenthesis in Eq. (8), is a smooth positive function of ω. We therefore conclude that the main contribution to $\bar{\mathcal{I}}$ originates from a frequency range around transmission resonances, where $P(\omega)$ becomes significant due to the rapid changes of the instantaneous reflection phase α^t and reflectance R^t. In the case of near-field resonant thermal transport, these resonances are associated with the poles of the scattering matrix equation (3). When a pair of nearby resonances approach one another, they can further enchance the sensitivity of α^t and R^t on the parameters of the pump, thus increasing the pumping-induced thermal energy flux density $\bar{\mathcal{I}}$. Below, we demonstrate how one can engineer such a scenario by utilizing the existence of a DP degeneracy.

A prototype CMT model and parametric analysis of eigenmodes of the effective Hamiltonian.—We consider a prototype system of three coupled resonant modes that supports a DP degeneracy. The isolated system is described by the instantaneous CMT Hamiltonian

$$H_0^t = \begin{bmatrix} \omega_0 + v^t & -1 & 1 \\ -1 & \omega_0 & -1 \\ 1 & -1 & \omega_0 + u^t \end{bmatrix}. \quad (9)$$

When $u^t = v^t = 0$, the eigenfrequencies of H_0^t are $a_1^{(0)} = a_2^{(0)} = \omega_{\rm DP} = \omega_0 - 1$ (DP degeneracy) and $a_3^{(0)} = \omega_0 + 2$. In the neighborhood of the DP degeneracy, we can invoke a degenerate perturbation theory in order to analyze the eigenfrequency spectrum. Specifically, the projection of H_0^t in the degenerate eigenspace $\{|a_1^{(0)}\rangle, |a_2^{(0)}\rangle\}$ is the 2×2 Hamiltonian $H_0^{t,(2)}$ [42],

$$H_0^{t,(2)} = g_0 I_2 + g_x\sigma_x + g_z\sigma_z, \quad (10)$$

where σ_x, σ_z are the Pauli matrices, $g_0 = \omega_0 - 1 + \frac{1}{3}(u^t + v^t)$, $g_x = (u^t - v^t)/(2\sqrt{3})$, and $g_z = \frac{1}{6}(u^t + v^t)$. Therefore, the eigenvalue spectrum of H_0^t around $\omega_{\rm DP}$ is approximated by the eigenvalues of $H_0^{t,(2)}$. The latter are $a_{1,2}^t \approx g_0 \pm \sqrt{g_x^2 + g_z^2} = \omega_0 - 1 + \frac{1}{3}(u^t + v^t) \pm \frac{1}{2\sqrt{3}}\sqrt{(u^t - v^t)^2 + \frac{1}{3}(u^t + v^t)^2}$, indicating that when (u^t, v^t) move away from (0,0) along an arbitrary line $u^t \propto v^t$, the eigenfrequency splitting is linear; see Fig. 2(a). The associated conical intersection signifies the presence of a DP, i.e., a spectral degeneracy where the Hamiltonian possesses two linearly independent eigenvectors [31].

When the isolated system of Eq. (9) is coupled to leads, the eigenfrequency surfaces "evolve" to resonance surfaces. The associated resonant frequencies are the real parts of the poles of the S-matrix which are identified with the complex eigenvalues $\{a_n\}$ of the effective Hamiltonian $H_{\rm eff}^t = H_0^t + \Lambda - (i/2)\hat{W}\hat{W}^T$. For simplicity, we assume a wide-band approximation [42]. In the weak coupling limit $|\varepsilon| \to 0$ and when (u^t, v^t) vary around (0,0), we can employ a similar analysis as before. Specifically, $H_0^{t,(2)} \to H_{\rm eff}^{t,(2)}$ via the substitution in Eq. (10) of $(g_0, g_z) \to (g_0 - \frac{2}{3}\imath\varepsilon^2,\ g_z \to g_z - \frac{1}{3}\imath\varepsilon^2)$. Diagonalization of $H_{\rm eff}^{t,(2)}$ for $\epsilon \neq 0$ indicates that the DP split into two exceptional points (EPs), emerging at $(u^t, v^t) = (1/\sqrt{3})\varepsilon^2(1, -1)$ and $(1/\sqrt{3})\varepsilon^2(-1, 1)$; see Fig. 2(b). A characteristic signature of the EP singularity is the fact that the degeneracy lifting

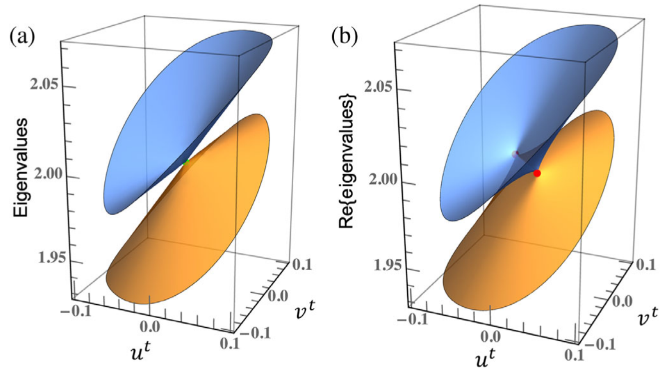

FIG. 2. Eigenvalue surfaces of the effective Hamiltonian $H_{\rm eff}^t$ around $\omega_{\rm DP} = \omega_0 - 1$, when (a) the coupling strength $\varepsilon = 0$, and (b) $\varepsilon = -0.2$. When the system is coupled to leads, the DP [indicated by the green dot in (a)] evolves into two EPs; see the red dots in (b). Another common parameter is $\omega_0 = 3$.

follows a square root behavior with respect to the distance from the EP. For example, around the EP $(u^t, v^t) = (1/\sqrt{3})\epsilon^2(1,-1)$, we have an eigenvalue splitting $a_1^t - a_2^t \approx -(2\sqrt{2}/3)e^{-\imath\pi/12}\epsilon\sqrt{u^t - (1/\sqrt{3})\epsilon^2}$ when fixing $v^t = -(1/\sqrt{3})\epsilon^2$ and varying u^t.

At parameter values (u^t, v^t) corresponding to the line $u^t + v^t = 0$ which connects the two EPs, the eigenvalues of the system take the form $a_{1,2}^t \approx \omega_0 - 1 - \frac{2}{3}\imath\epsilon^2 \pm (1/\sqrt{3})\sqrt{(u^t)^2 - \frac{1}{3}\epsilon^4}$. On the line $u^t + v^t = 0$, when $|u^t| \le (1/\sqrt{3})\epsilon^2$, the real part of the eigenvalues are degenerate; see Fig. 2(b). The presence of this resonance degenerate line (RDL) imposes a sense of directionality in the $u^t - v^t$ parameter space, and "enforces" a detailed analysis of pumping for small cycles centered along and perpendicular to it. In fact, this argument predicts that driving cycles placed symmetrically in the $u^t - v^t$ plane with respect to the RDL will lead to the same behavior of $\bar{\mathcal{I}}$ [42].

Examples of adiabatic pumps.—In our examples, we parametrize the pumping circle in Eq. (9) as $u^t = u^{(0)} + \delta u^t$, $v^t = v^{(0)} + \delta v^t$ with $(u^{(0)}, v^{(0)}) = (d\cos\theta, d\sin\theta)$ and $\delta u^t = \delta u^{t+2\pi/\Omega}$, $\delta v^t = \delta v^{t+2\pi/\Omega}$. The pair $(u^{(0)}, v^{(0)})$ determines the center of the adiabatic cycle, and it is reparametrized with θ and d in polar representation. We also assume tight-binding leads with dispersion $\omega = \omega_0 - 2\cos k$ that are coupled to the scattering target with coupling constants $w_L = w_R = \epsilon$.

First, we choose $\theta = 45^0$, $\delta u^t = r\cos\Omega t$, and $\delta v^t = r\sin\Omega t$, corresponding to a pumping cycle with a center along the line perpendicular to the RDL. The latter is embedded in the plane $\omega = \omega_{\rm DP} = \omega_0 - 1$; see Fig. 2(b). In Fig. 3(a), we report the numerical calculations for $\bar{\mathcal{I}}$ evaluated using Eqs. (4) and (6). In fact, one can derive analytically the following expression for the total radiative (time-averaged) energy flux $\bar{\mathcal{I}}$ per pumping area [42]

$$\tilde{\mathcal{I}} \approx \frac{\Omega}{2\pi}\left(\hbar\omega\frac{\partial\Theta_T(\omega)}{\partial k}\right)_{\omega_{\rm DP}} \frac{4\sqrt{3}\epsilon^4(\epsilon^2 - \sqrt{2}d)}{[(\epsilon^2 - \sqrt{2}d)^2 + 12\epsilon^4]^2}, \tag{11}$$

which nicely matches the numerics; see Fig. 3(a). Equation (11) is obtained from Eq. (8) using the residue theorem. Essentially, it describes the contribution of two terms, i.e.,

$$\bar{\mathcal{I}} \propto \sum_{n\in\text{pair}} \text{Res}[P(\omega); \omega_n], \tag{12}$$

where $\text{Res}(\cdot)$ indicates the residue. The summation is over a pair of $P(\omega)$ poles near the DP, which are associated with the intersection of the vertical line $(u^t, v^t, \omega) = (u^{(0)}, v^{(0)}, \omega)$ with each of the two resonant surfaces shown in Fig. 2 [42]. The contributions of these two resonance surfaces appear to be the opposite of each other. It turns out that on each side of the RDL, either the upper or the lower resonance surface dominates the summation for the total current, leading to a net current which is either positive or negative; see Fig. 3(a). In contrast, when the center of the cycle moves far away from the RDL, both contributions diminish and the net current approaches zero. In this limit, the Hamiltonian H_0^t of the isolated system does not support a DP.

On the other hand, in the vicinity of the degenerate line, the contributions of the two resonant surfaces to $\bar{\mathcal{I}}$ change abruptly. At some critical distance $d = 0.007$, they balance one another and result in a zero net current; see Fig. 3(a). At $d = 0$, the two resonance surfaces merge, and therefore the summation collapses to one term, leading to a large value of the net current $\bar{\mathcal{I}}$. In fact, the last argument is also applicable to the case of $\theta = 135^0$, corresponding to a pumping cycle whose center moves along the RDL. In this case, the net current acquires large values for $d \approx 0$, while it diminishes symmetrically as $|d|$ increases; see Fig. 3(b). We point out that the extrema of $\bar{\mathcal{I}}$ appears always in the *vicinity* of the DP corresponding to $H_0^t(d = 0; r = 0)$. Furthermore, when the coupling to the leads $|\epsilon|$ increases, the DP degeneracy is lifted, and thus the performance of the pump deteriorates; see Fig. 3. For further details and other values of θ, see the Supplemental Material [42].

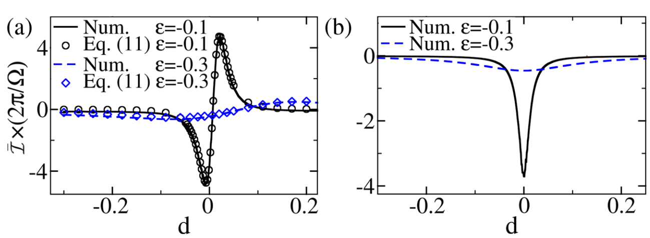

FIG. 3. Numerical evaluation (dashed lines) of rescaled radiative (time-averaged) thermal energy flux $\bar{\mathcal{I}} \times (2\pi/\Omega)$ versus the control parameter d for driving angles (a) $\theta = 45°$ and (b) $\theta = 135°$. The coupling ϵ between the leads and the system is indicated in the insets. In (a), we also report the theoretical result (symbols) of Eq. (11). Other parameters are $k_BT/\hbar = 1.25$ and $\omega_0 = 3$ (in units of coupling strength).

Adiabatic pumping using circuits.—An experimental demonstration of the effects of DPs on the adiabatically pumped thermal radiation can be achieved using the electrical circuit shown in Fig. 1(b) [42]. The reservoirs are represented by a model for bandwidth limited Thevenin equivalent TEM transmission lines with characteristic impedance $Z_0 = 50\ \Omega$. The noise sources V_n are synthesized such that $\langle V_n(\omega)V_m^*(\omega')\rangle = (2Z_0/\pi)\Phi(\omega)\delta(\omega - \omega')\delta_{nm}$, where $\Phi(\omega) = k_BT\Theta(\omega)$. For demonstration purposes, we set $\Theta(\omega) = \sqrt{1 - (\omega/2\omega_c)^2}$, with $\omega_c \approx 0.47$ GHz. The pumping scheme is chosen to always enclose a DP [42]. Specifically, we consider a

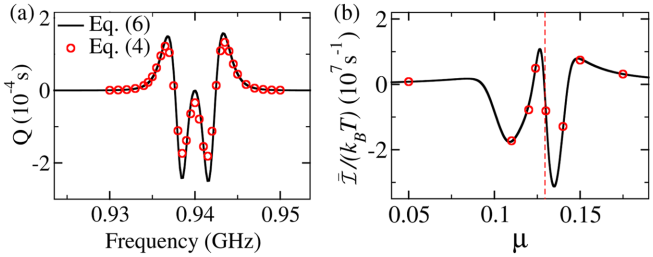

FIG. 4. (a) Total pumped energy density $Q(\omega)$ versus frequency for a typical value of the rescaled mutual inductance coupling at the DP, $\mu = \mu_{\mathrm{DP}}$. (b) Total (averaged) pumped radiative energy current $\hat{\mathcal{I}}$ versus the mutual inductance μ. The highest values of $\hat{\mathcal{I}}$ are reached at the proximity of the DP (red dashed line). (a),(b) The lines are obtained from the numerical evaluation of $Q(\omega)$ using Eq. (6). The symbols are results from a direct time-domain simulation of net power at the left terminal [50].

periodic modulation of the capacitances at left and right resonators such that $C_1(t) = C[1 + r\sin(\Omega t)]$, $C_2(t) = C[1 + r\cos(\Omega t)]$.

Next, we inject into the circuit uncorrelated incoming waves of the same frequency ω and power $P_s = V_s^2/(8Z_0)$ from the left (L) and right (R) reservoir. The average (over a cycle) net power flowing through the node L (R) is obtained from the voltage $v_{L(R)}(t)$ and current $i_{L(R)}(t)$ sampled at the respective node L (R) [42]. Specifically, $Q(\omega)$ is evaluated using Eq. (4), where the time-dependent energy current is $\mathcal{I}_{L(R)}(t,\omega) = v_{L(R)}(t,\omega) i_{L(R)}(t,\omega)/P_s$. In our simulations, we made sure that the system reached a stationary state before the evaluation. The results from the time-domain simulations are shown in Fig. 4(a) together with the outcome from the instantaneous S^t-matrix approach; see Eq. (6).[50] In the latter case, we have extracted the instantaneous reflectance R^t and reflection phase α^t using a standard scattering approach (see the Supplemental Material [42]) [51].

Having at our disposal the total radiative energy density $Q(\omega)$ for the circuit setup, we are now able to incorporate $\Phi(\omega)$ for the radiative thermal energy flux (per pumping area) passing through the system, $\bar{\mathcal{I}}$ versus μ. In Fig. 4(b), we report our findings using the instantaneous S^t matrix and the direct time-domain approaches. The data nicely demonstrate the enhancement in $\bar{\mathcal{I}}$ due to the presence of the DP, as expected from the predictions of CMT.

Conclusions.—We introduced the concept of adiabatic thermal radiation pumps as a means to manage the direction of net radiative energy current between bodies in equilibrium. We addressed this problem by appropriately adopting, and establishing in the framework of resonant near-field thermal radiation, an instantaneous scattering matrix formalism. Using this tool, we highlighted the importance of wave interference effects and demonstrated the impact of DP spectral singularities in thermal radiation management. Our results have been tested against realistic simulations using electronic circuits. An exciting application of our proposal might involve tunable superconducting resonators [52,53], which will enable new forms of superconducting Q-bit manipulation. A future interesting direction is the study of the full counting statistics for thermal radiation. These questions will be addressed in a subsequent study.

H. L., L. J. F.-A., and T. K. acknowledge partial support from ONR Grant No. N00014-16-1-2803, from the DARPA NLM program via Grant No. HR00111820042, and from AFOSR Grant No. FA 9550-14-1-0037. B. S. acknowledges the hospitality of Wesleyan University, where this work was performed.

*H. L. and L. J. F.-A. contributed equally to this work.

[1] A. Volokitin and B. Persson, Near-field radiative heat transfer and noncontact friction, Rev. Mod. Phys. **79**, 1291 (2007).
[2] J. R. Howell, R. Siegel, and M. P. Mengüs, *Thermal Radiation Heat Transfer*, 5th ed. (CRC Press, Boca Raton, FL, 2010).
[3] T. L. Bergman, A. S. Lavine, F. P. Incropera, and D. P. Dewitt, *Introduction to Heat Transfer*, 6th ed. (Wiley, Hoboken, NJ, 2011).
[4] S. Fan, Thermal photonics and energy applications, Joule **1**, 264 (2017).
[5] D. A. B. Miller, L. Zhu, and S. Fan, Universal modal radiation laws for all thermal emitters, Proc. Natl. Acad. Sci. U.S.A. **114**, 4336 (2017).
[6] L. Zhu and S. Fan, Near-complete violation of detailed balance in thermal radiation, Phys. Rev. B **90**, 220301(R) (2014).
[7] W. C. Snyder, Z. Wan, and X. Li, Thermodynamic constraints on reflectance reciprocity and Kirchoff's law, Appl. Opt. **37**, 3464 (1998).
[8] Y. Hadad, J. C. Soric, and A. Alú, Breaking temporal symmetries for emission and absorption, Proc. Natl. Acad. Sci. U.S.A. **113**, 3471 (2016).
[9] A. W. Rodriguez, O. Ilic, P. Bermel, I. Celanovic, J. D. Joannopoulos, M. Soljacic, and S. G. Johnson, Frequency-Selective Near-Field Radiative Heat Transfer between Photonic Crystal Slabs: A Computational Approach for Arbitrary Geometries and Materials, Phys. Rev. Lett. **107**, 114302 (2011).
[10] P. Ben-Abdallah and S.-A. Biehs, Near-Field Thermal Transistor, Phys. Rev. Lett. **112**, 044301 (2014).
[11] S. Shen, A. Narayanaswamy, and G. Chen, Surface phonon polaritons mediated energy transfer between nanoscale gaps, Nano Lett. **9**, 2909 (2009).
[12] E. Rousseau, A. Siria, G. Jourdan, S. Volz, F. Comin, J. Chevrier, and J.-J. Greffet, Radiative heat transfer at the nanoscale, Nat. Photonics **3**, 514 (2009).
[13] R. S. Ottens, V. Quetschke, S. Wise, A. A. Alemi, R. Lundock, G. Mueller, D. H. Reitze, D. B. Tanner, and B. F. Whiting, Near-Field Radiative Heat Transfer between Macroscopic Planar Surfaces, Phys. Rev. Lett. **107**, 014301 (2011).
[14] T. Kralik, P. Hanzelka, M. Zobac, V. Musilova, T. Fort, and M. Horak, Strong Near-Field Enhancement of Radiative

Heat Transfer between Metallic Surfaces, Phys. Rev. Lett. **109**, 224302 (2012).
[15] R. St-Gelais, B. Guha, L. Zhu, S. Fan, and M. Lipson, Demonstration of strong near-field radiative heat transfer between integrated nanostructures, Nano Lett. **14**, 6971 (2014).
[16] J. Shi, B. Liu, P. Li, L. Y. Ng, and S. Shen, Near-field energy extraction with hyperbolic metamaterials, Nano Lett. **15**, 1217 (2015).
[17] K. Kim, B. Song, V. Fernandez-Hurtado, W. Lee, W. Jeong, L. Cui, D. Thompson, J. Feist, M. T. H. Reid, F. J. Garciá-Vidal, J. C. Cuevas, E. Meyhofer, and P. Reddy, Radiative heat transfer in the extreme near field, Nature (London) **528**, 387 (2015).
[18] B. Song, Y. Ganjeh, S. Sadat, D. Thompson, A. Fiorino, V. Fernandez-Hurtado, J. Feist, F. J. Garcia-Vidal, J. C. Cuevas, P. Reddy, and E. Meyhofer, Enhancement of near-field radiative heat transfer using polar dielectric thin films, Nat. Nanotechnol. **10**, 253 (2015).
[19] R. St-Gelais, L. Zhu, S. Fan, and M. Lipson, Near-field radiative heat transfer between parallel structures in the deep subwavelength regime, Nat. Nanotechnol. **11**, 515 (2016).
[20] B. Song, D. Thompson, A. Fiorino, Y. Ganjeh, P. Reddy, and E. Meyhofer, Radiative heat conductances between dielectric and metallic parallel plates with nanoscale gaps, Nat. Nanotechnol. **11**, 509 (2016).
[21] S. Y. Lin, J. Moreno, and J. G. Fleming, Three-dimensional photonic-crystal emitter for thermal photovoltaic power generation, Appl. Phys. Lett. **83**, 380 (2003).
[22] A. Narayanaswamy and G. Chen, Surface modes for near field thermophotovoltaics, Appl. Phys. Lett. **82**, 3544 (2003).
[23] S. Basu, Z. M. Zhang, and C. J. Fu, Review of near-field thermal radiation and its application to energy conversion, Int. J. Energy Res. **33**, 1203 (2009).
[24] O. Ilic, M. Jablan, J. D. Joannopoulos, I. Celanovic, and M. Soljacic, Overcoming the black body limit in plasmonic and graphene near-field thermophotovoltaic systems, Opt. Express **20**, A366 (2012).
[25] Y. De Wilde, F. Formanek, R. Carminati, B. Gralak, P.-A. Lemoine, K. Joulain, J.-P. Mulet, Y. Chen, and J.-J. Greffet, Thermal radiation scanning tunnelling microscopy, Nature (London) **444**, 740 (2006).
[26] A. Kittel, W. Müller-Hirsch, J. Parisi, S.-A. Biehs, D. Reddig, and M. Holthaus, Near-Field Heat Transfer in a Scanning Thermal Microscope, Phys. Rev. Lett. **95**, 224301 (2005).
[27] C. R. Otey, W. Tung Lau, and S. Fan, Thermal Rectification Through Vacuum, Phys. Rev. Lett. **104**, 154301 (2010).
[28] S. Basu and M. Francoeur, Near-field radiative transfer based thermal rectification using doped silicon, Appl. Phys. Lett. **98**, 113106 (2011).
[29] L. Zhu, C. R. Otey, and S. Fan, Negative differential thermal conductance through vacuum, Appl. Phys. Lett. **100**, 044104 (2012).
[30] B. Guha, C. Otey, C. B. Poitras, S. Fan, and M. Lipson, Near-field radiative cooling of nanostructures, Nano Lett. **12**, 4546 (2012).
[31] M. V. Berry and M. Wilkinson, Diabolical points in the spectra of triangles, Proc. R. Soc. A **392**, 15 (1984).
[32] P. W. Brouwer, Scattering approach to parametric pumping, Phys. Rev. B **58**, R10135 (1998).
[33] D. J. Thouless, Quantization of particle transport, Phys. Rev. B **27**, 6083 (1983).
[34] B. L. Altshuler and L. I. Glazman, Pumping electrons, Science **283**, 1864 (1999).
[35] O. Entin-Wohlman, A. Aharony, and Y. Levinson, Adiabatic transport in nanostructures, Phys. Rev. B **65**, 195411 (2002).
[36] J. E. Avron, A. Elgart, G. M. Graf, and L. Sadun, Optimal Quantum Pumps, Phys. Rev. Lett. **87**, 236601 (2001).
[37] D. Cohen, Quantum pumping and dissipation: From closed to open systems, Phys. Rev. B **68**, 201303(R) (2003).
[38] M. Switkes, C. M. Marcus, K. Campman, and A. C. Gossard, An adiabatic quantum electron pump, Science **283**, 1905 (1999).
[39] L. Zhu, S. Sandhu, C. Otey, S. Fan, M. B. Sinclair, and T. S. Luk, Temporal coupled mode theory for thermal emission from a single thermal emitter supporting either a single mode or an orthogonal set of modes, Appl. Phys. Lett. **102**, 103104 (2013).
[40] A. Karalis and J. D. Joannopoulos, Temporal coupled-mode theory model for resonant near-field thermophotovoltaics, Appl. Phys. Lett. **107**, 141108 (2015).
[41] H. Li, S. Suwunnarat, R. Fleischmann, H. Schanz, and T. Kottos, Random Matrix Theory Approach to Chaotic Coherent Perfect Absorbers, Phys. Rev. Lett. **118**, 044101 (2017).
[42] See Supplemental Material at http://link.aps.org/supplemental/10.1103/PhysRevLett.123.165901, which includes Refs. [31,35,43], for a detailed derivation and further analysis.
[43] K. Fang, Z. Yu, and S. Fan, Photonic Aharonov-Bohm Effect Based on Dynamic Modulation, Phys. Rev. Lett. **108**, 153901 (2012).
[44] Note that $Q(\omega)$ does not depend on the position x_0 where the flux is evaluated because, on average, no net energy is accumulated in the setup.
[45] Y. Levinson, O. Entin-Wohlman, and P. Wolfle, Pumping at resonant transmission and transferred charge quantization, Physica (Amsterdam) **302A**, 335 (2001).
[46] O. Entin-Wohlman and A. Aharony, Quantized adiabatic charge pumping and resonant transmission, Phys. Rev. B **66**, 035329 (2002).
[47] M. Blaauboer, Charge pumping in mesoscopic systems coupled to a superconducting lead, Phys. Rev. B **65**, 235318 (2002).
[48] T. A. Shutenko, I. L. Aleiner, and B. L. Altshuler, Mesoscopic fluctuations of adiabatic charge pumping in quantum dots, Phys. Rev. B **61**, 10366 (2000).
[49] I. L. Aleiner and A. V. Andreev, Adiabatic Charge Pumping in Almost Open Dots, Phys. Rev. Lett. **81**, 1286 (1998).
[50] Circuit simulations were performed using NGSPICE v.28 plus, http://ngspice.sourceforge.net/.
[51] Z. Lin, J. Schindler, F. Ellis, and T. Kottos, Experimental observation of the dual behavior of PT-symmetric scattering, Phys. Rev. A **85**, 050101(R) (2012).
[52] A. A. Adamyan, S. E. Kubatkin, and A. V. Danilov, Tunable superconducting microstrip resonators, Appl. Phys. Lett. **108**, 172601 (2016).
[53] C. Bockstiegel, Y. Wang, M. R. Vissers, L. F. Wei, Chaudhuri, Hubmayr, and J. Gao, A tunable coupler for superconducting microwave resonators using a nonlinear kinetic inductance transmission line, Appl. Phys. Lett. **108**, 222604 (2016).